

# Physical picture for fractures in stratified materials: viscoelastic effects in large cracks

Ko Okumura\*

*Physique de la Matière Condensée,*

*Collège de France,*

*11 place Marcelin-Berthelot,*

*75231 Paris cedex 05, France*

*and*

*Department of Physics,*

*Graduate School of Humanities and Sciences,*

*Ochanomizu University,*

*2-1-1, Otsuka, Bunkyo-ku,*

*Tokyo 112-8610, Japan*

(Dated: October 29, 2018)

## Abstract

We present an intuitive physical picture for fractures in nacre-type stratified materials via scaling arguments: strain distributions around a fracture are rather different depending on directions and size of fractures. We thus observe that viscoelastic effects are important for parallel fractures. This effect are taken into account via the simplest viscoelastic model for weakly cross-linked polymer. Within a certain limit, we find a trumpet crack shape similar to that in certain polymers and make predictions for the fracture energy of certain stratified materials in this mode.

---

\*Electronic address: okumura@phys.ocha.ac.jp

## I. INTRODUCTION

Strong structures created in nature through a long history of natural selection sometimes take advantage of composite structures such as laminar structures (tooth, timber etc.) where soft and hard layers are intertwined. Biomimetics aims at exploiting such ideas and some industrial materials (from blockboard to high-tech tires) have utilized the concept of stacking lamellae to enhance their toughness [1, 2, 3, 4, 5]. In a series of papers [6, 7, 8], we have studied another example of such soft-hard laminar structure on nanoscales, *nacre* [9, 10, 11, 12], to present physical pictures for this substance.

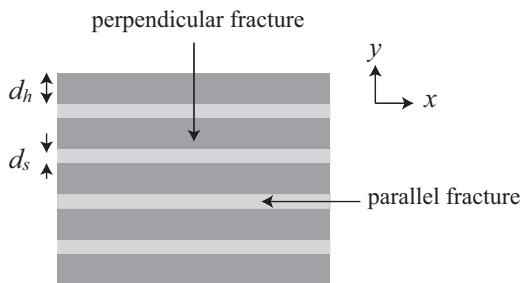


FIG. 1: Nacre-type structure of materials: hard layers (the elastic modulus  $E_h$ ) has a typical thickness  $d_h$ , which are glued together by soft layers (the elastic modulus  $E_s$ ) of a typical thickness  $d_s$ . An important conditions for these parameters are  $\varepsilon_0 = E_s/E_h, \varepsilon_d = d_s/d_h \ll 1$  with  $\varepsilon = \varepsilon_0/\varepsilon_d \ll 1$ . The cracks in the  $y - z$  plane and the  $x - z$  plane are called a perpendicular and parallel fractures, respectively (the  $z$ -axis is perpendicular to this page).

The structure and notations are illustrated in Fig. 1. A typical thickness  $d_s$  of the soft layer made from a protein, *conchiolin*, is dozens of nanometer, which is much smaller than a micrometric thickness  $d_h$  of the hard layer composed of *aragonite*. An elastic modulus  $E_s$  of the soft layer is also much smaller than  $E_h$  of the hard layer where the latter is roughly given by 50 GPa. We define two small quantities:

$$\varepsilon_d = d_s/d_h \tag{1}$$

$$\varepsilon_0 = E_s/E_h \tag{2}$$

An important property of nacre is that  $\varepsilon$  defined by

$$\varepsilon \equiv \varepsilon_0/\varepsilon_d \tag{3}$$

is very small. We will work in the limit of  $\varepsilon_0, \varepsilon_d, \varepsilon \ll 1$ , and also in the continuum limit where relevant length scales are much larger than the layer spacing  $d$ :

$$d = d_s + d_h. \quad (4)$$

We emphasize here that under these conditions our theory is applicable to a general layered structure other than nacre. Physically,  $\varepsilon_d$  *has to be small to make a relatively ridged material (as a whole)*, while  $\varepsilon$  (and thus  $\varepsilon_0$ ) *has to be small to make the stress concentration around tip small to enhance the toughness*; these conditions seem to have been indeed selected in nacre by nature.

We have been studied both perpendicular and parallel fractures (see Fig. 1) within the linear elastic fracture mechanics (LEFM [13]) under the plain strain condition (the sample is thick in the  $z$ -direction) [6, 7, 8]. One of our aims here is to include a linear viscoelastic effect into this system.

## II. NOVEL VIEWS ON PREVIOUS RESULTS

The proposed elastic energy per unit volume of the stratified system is given by [7]

$$f = E_h e_{xx}^2 + E_0 e_{yy}^2 + E_0 e_{xy}^2 + E_0 e_{xx} e_{yy} \quad (5)$$

where

$$E_0 = \varepsilon E_h, \quad (6)$$

We have introduced the strain field

$$e_{ij} = \frac{1}{2} \left( \frac{\partial u_i}{\partial x_j} + \frac{\partial u_j}{\partial x_i} \right) \quad (7)$$

for the deformation field  $u_i$  where  $(x_1, x_2, x_3) = (x, y, z)$ . This energy reflects, via  $\sigma_{ij} = \partial f / \partial e_{ij}$ , intuitively self-evident properties that (1) this system is hard for a tensile stress in the  $x$ -direction ( $\sigma_{xx} \simeq E_h e_{xx}$ ) due to hard layers, (2) it is soft for a tensile stress in the  $y$ -direction ( $\sigma_{yy} \simeq E_0 e_{yy}$ ) due to soft layers, and (3) it is soft for a shear stress ( $\sigma_{xy} \simeq E_0 e_{xy}$ ) again due to soft layers. Here, we notice that the effectiveness of soft layers is diminished ( $E_s \rightarrow E_0$ ) by the thin thickness of the soft layers.

For parallel fractures, we have shown that a usually negligible bending term becomes important [8], which shall be confirmed below from a different viewpoint. The bending term

is given by

$$f_B = K_B \left( \frac{\partial^2 u_y}{\partial x^2} \right)^2 \quad (8)$$

where

$$K_B = E_h d^2 \equiv E_0 l^2. \quad (9)$$

Here we have introduced a length scale,

$$l = d/\sqrt{\varepsilon}, \quad (10)$$

which is much longer than the layer period  $d$ . This bending term becomes important also in certain liquid crystals [14, 15]. However, there is a significant difference from the present situation; in liquid crystals  $l$  is replaced by a much smaller length of the order of atomic scales, which results in a strain distribution quite different from nacre (see below).

### A. Scaling structure of elastic energy

An important difference from the conventional isotropic elastic theory is that, in an anisotropic system such as nacre, there exist two distinct length scales  $X$  and  $Y$ . On the contrary, in isotropic systems at equilibrium when the elastic body is deformed over a range of  $R$  in the  $x$ -direction, the deformation relaxes out at the same distance  $R$  also in the  $y$ -direction; this is because the deformation field of an isotropic system satisfies an elliptic differential equation with a unique length scale (under the plain strain condition). In other words, the deformation in nacre does not satisfy the Laplace equation. Note here that, in the context of a fracture problem,  $X$  corresponds to a length of parallel fracture while  $Y$  to that of perpendicular fracture (see Fig. 2 below).

Thus, a local energy (per unit volume) of nacre is dimensionally expressed as

$$\begin{aligned} f \simeq & E_h \left( \frac{u_x}{X} \right)^2 + E_0 \left( \frac{u_y}{Y} \right)^2 \\ & + E_0 \left( \frac{u_x}{Y} + \frac{u_y}{X} \right)^2 + E_0 \frac{u_x}{X} \cdot \frac{u_y}{Y} + K_B \left( \frac{u_y}{X^2} \right)^2 \end{aligned} \quad (11)$$

At equilibrium (statics),  $f$  is locally minimized for both variables  $u_x$  and  $u_y$ ; we have two equations for  $u_x$  and  $u_y$ , i.e.  $\partial f/\partial u_x = 0$  and  $\partial f/\partial u_y = 0$ . Seeking the relevant solution by requiring  $(u_x, u_y) \neq (0, 0)$ , we have an equation for  $X$  and  $Y$ . This equation has two solutions specifying a relation between  $X$  and  $Y$ ; one corresponds to perpendicular fractures while

the other to parallel fractures. We should note that here and hereafter a limitation of this type of dimensional expressions: relative signs (or phases of complex numbers) sometimes can not be specified.

### 1. Parallel fractures

The solution for parallel fractures announces a relation,  $X^2 \simeq Y^2(1 + l^2/X^2)$ , which implies two regimes for this problem:  $X \gg l$  and  $X \ll l$ .

For large fractures ( $X \gg l$ ), we have an isotropic relation,

$$X \simeq Y. \quad (12)$$

On the other hand, with an aide of a relation  $\partial f/\partial u_x = 0$  together with Eq. (12), we obtain an anisotropic deformation field,

$$u_x \simeq \varepsilon u_y; \quad (13)$$

we find  $u_x \ll u_y$ , which is appropriate for parallel fractures. Using Eqs. (12) and (13), we can estimate magnitudes of each term in Eq. (11). Keeping terms only at the leading order in  $\varepsilon$ , we arrive at

$$f \simeq E_0 \left( \frac{u}{R} \right)^2 \quad (14)$$

where we denote scales of  $X$  ( $\simeq Y$ ) and  $u_y$  as  $R$  and  $u$ , respectively. This corresponds to a more precise form  $f \simeq E_0 \left( \frac{\partial u_y}{\partial y} \right)^2 + E_0 \left( \frac{\partial u_y}{\partial x} \right)^2$  shown in [7].

For small fractures ( $X \ll l$ ), we have instead

$$X^2 \simeq Yl, \quad (15)$$

which implies  $X \gg Y$ . The deformation field satisfies

$$u_x \simeq \frac{l}{X} \varepsilon u_y \quad (16)$$

Here, we note an important condition for a continuum theory:  $X, Y > d$ . This condition, together with Eq. (10), results in

$$\varepsilon l^2/X^2, \varepsilon l^2/Y^2 < 1 \quad (17)$$

which implies  $\varepsilon l/X, \varepsilon l/Y < \sqrt{\varepsilon} \ll 1$  (note also that this does not necessarily imply  $l < X, Y$ ; e.g.  $X \gtrsim \sqrt{\varepsilon}l$  satisfies both  $l > X$  and  $\varepsilon l/X < 1$ ). Thus, we again find  $u_x \ll u_y$ . In this

way, we arrive at

$$f \simeq E_0 \left( \frac{u}{Y} \right)^2 \simeq K_B \left( \frac{u}{X^2} \right)^2 \quad (18)$$

which corresponds to  $f \simeq E_0 \left( \frac{\partial u_y}{\partial y} \right)^2 + K_B \left( \frac{\partial^2 u_y}{\partial x^2} \right)^2$  shown in [8].

## 2. Perpendicular fractures

The solution for perpendicular fractures announces an anisotropic relations,

$$Y \simeq \sqrt{\varepsilon} X \quad (19)$$

$$u_y \simeq \sqrt{\varepsilon} u_x \quad (20)$$

for which  $u_x \gg u_y$ . These relations lead to an energy,

$$f \simeq E_h \left( \frac{u}{X} \right)^2 \simeq E_0 \left( \frac{u}{Y} \right)^2. \quad (21)$$

Here,  $u$  denotes not  $u_y$  but  $u_x$ . This energy corresponds to  $f \simeq E_h \left( \frac{\partial u_x}{\partial x} \right)^2 + E_0 \left( \frac{\partial u_x}{\partial y} \right)^2$  shown in [7].

## B. Scaling views on fracture mechanics

We consider a fracture in nacre-type materials. Strain distribution for three types of fractures are schematically given in Fig. 2. We should note that these figures are *at the scaling level* and thus they are rather rough images; some examples of comparison with exact results are given in Appendix. We will develop below scaling arguments in order to reproduce our previous results but only dimensionally. Similar arguments in a different context was first presented in [14].

### 1. Parallel fractures

For *large cracks* ( $X \gg l$ ), the strain distribution is isotropic (Fig. 2a) and, thus, the potential energy per unit crack-front length (in  $z$ -direction) is dimensionally given by

$$F \simeq E_0 \left( \frac{u}{R} \right)^2 R^2 - \sigma u R + 2G_{\parallel} R \quad (22)$$

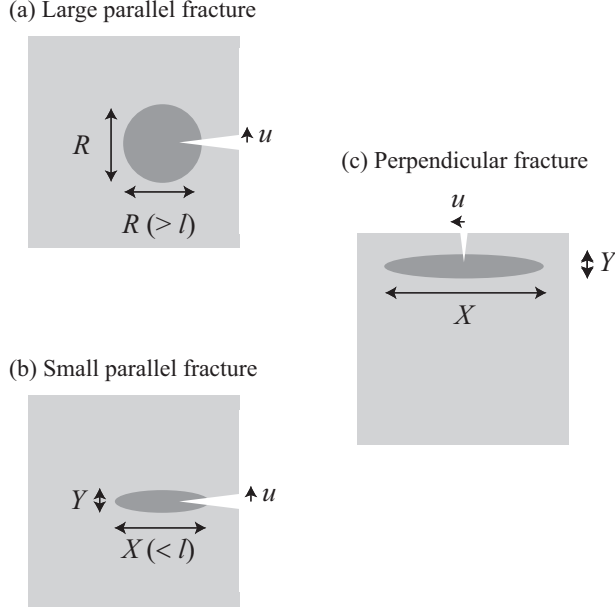


FIG. 2: Physical images of strain distribution accompanying a fracture. Dark areas indicate the region where the strain field is significant. (a) Large parallel fracture. There is only one length scale  $R (\gg l)$  for the distribution, where the crack length is also of the order of  $R$ . (b) Small parallel fracture. The strain distribution becomes rather anisotropic: the length scale  $X (\ll l)$  for  $x$ -direction is larger than  $Y$ , where the crack size is of the order of  $X$ . (c) Perpendicular fracture. An anisotropic strain distribution with  $X \gg Y$ , where the crack size is of the order of  $Y$ .

where the first two terms describes the elastic potential energy and the last term an energy loss due to a creation of new surfaces in this system:  $G_{\parallel}$  is the fracture energy (energy required to create a unit area). We minimize this energy with respect to  $u$  to find a Hooke's law

$$\sigma \simeq E_0 u / R \quad (23)$$

which leads to an optimized energy value,

$$F_m \simeq -\sigma^2 R^2 / E_0 + 2G_{\parallel} R, \quad (24)$$

which is quadratic in  $R$ ; the maximum is given at  $R = R^*$ :

$$\sigma \simeq \sqrt{G_{\parallel} E_0 / R^*}. \quad (25)$$

When  $R < R^*$ ,  $F_m$  decreases with decrease in  $R$ ; a fracture with the size smaller than  $R^*$  tends to close to lower the energy. On the contrary, when  $R > R^*$ ,  $F_m$  decreases with

increase in  $R$ ; a fracture with the size larger than  $R^*$  tends to expand. Thus, Eq. (25) corresponds to a critical failure stress. From Eqs. (23) and (25), we have

$$u \simeq \sqrt{G_{\parallel} R^* / E_0} \quad (26)$$

Eqs. (25) and (26) give scaling structures for the stress and deformation fields obtained more precisely in [7]: the stress scales as  $R^{-1/2}$  and the deformation is parabolic ( $\sim \sqrt{R}$ ) as in the conventional LEFM. They also give a scaling relation

$$\sigma u \simeq G_{\parallel}, \quad (27)$$

which announces that the product  $\sigma u$  (at critical state,  $R \simeq R^*$ ) gives the fracture energy (see Discussion). The fracture energy  $G_{\parallel}$  might be associated with the separation energy of the soft layer and we previously concluded that there was no significant enhancement in this mode. Due to the ensuing analysis we can afford a more precise understanding on this.

In conventional LEFM, the stress intensity factor  $K$  scales as  $\sqrt{\mathcal{G} E_0}$  in the present context where  $\mathcal{G}$  is *the energy release rate and its critical value* is the fracture energy ( $G_{\parallel}$ ). Eq. (25) suggests that  $K$  scales not as  $\sqrt{\mathcal{G} E_0}$  but as its critical value  $\sqrt{G_{\parallel} E_0}$ ; this is logical because in Eqs. (25)-(27) we are always at a critical of failure ( $R \simeq R^*$ ).

For *small cracks* ( $X \ll l$ ), the strain distribution is anisotropic (Fig. 2b). We note here that this distribution is quite different from certain cases of liquid crystals [14]; there strain is distributed more widely in  $y$ -direction than in  $x$ -direction. The potential of our system is given by

$$F \simeq K_B \left( \frac{u}{X^2} \right)^2 XY - \sigma u X + 2G_{\parallel} X. \quad (28)$$

We minimize this energy with respect to  $u$  to find a Hooke's law

$$\sigma \simeq E_0 u / Y \quad (29)$$

which corresponds to  $\sigma_{yy} \simeq E_0 \partial u_y / \partial y$ . Note here that the dominant component of stress field tensor is  $\sigma_{yy}$  (e.g.  $\sigma_{xy} \simeq E_0 \partial u_y / \partial x \simeq E_0 (u/X) \ll \sigma_{yy}$  due to Eq. (15)). The energy optimized for  $u$  is here given by

$$F_m \simeq -\sigma^2 X^3 l / K_B + 2G_{\parallel} X. \quad (30)$$

$F_m$  takes its maximum value at  $X \simeq X^* \simeq \sqrt{Y^*l}$ , where

$$\sigma \simeq \sqrt{\frac{K_B G_{\parallel}}{l}} \frac{1}{X^*} \simeq \sqrt{\frac{G_{\parallel} E_0}{Y^*}}, \quad (31)$$

$$u \simeq \sqrt{\frac{l G_{\parallel}}{K_B}} X^* \simeq \sqrt{\frac{G_{\parallel} Y^*}{E_0}}, \quad (32)$$

Eqs. (31) and (32) give scaling structures for the stress and deformation fields as well as a scaling relation  $\sigma u \simeq G_{\parallel}$ . We emphasize here that the stress thus obtained (which is proportional to strain) is indeed anisotropic;  $\sigma \sim 1/X \sim 1/\sqrt{Yl}$ . The stress and deformation fields obtained in [8] are also consistent with these scaling structures; we can check that, dimensionally,  $\sigma(x, y)$  and  $u(x, y)$  derived in [8] indeed reduce to Eqs. (31) and (32) by setting  $x^2 \simeq yl$  (because we are always in the regime specified by Eq. (15) at the scaling level).

## 2. Perpendicular fractures

The strain distribution is anisotropic (Fig. 2c) and, thus, the potential is given by

$$F \simeq E_h \left( \frac{u}{X} \right)^2 XY - \sigma u Y + 2G_{\perp} Y, \quad (33)$$

where  $G_{\perp}$  is the fracture energy. We minimize this energy with respect to  $u$  to find a Hooke's law

$$\sigma \simeq E_h u / X \quad (34)$$

which corresponds to  $\sigma_{xx} \simeq E_h \partial u_x / \partial x$  (the dominant stress tensor component in this case is  $\sigma_{xx}$ ). The energy optimized for  $u$  is here given by

$$F_m \simeq -\frac{\sigma^2 Y^2}{\sqrt{\varepsilon} E_h} + 2G_{\perp} Y. \quad (35)$$

$F_m$  takes its maximum value at  $Y \simeq Y^* \simeq \sqrt{\varepsilon} X^*$ , where

$$\sigma \simeq \sqrt{\frac{G_{\perp} E_h}{Y^* / \sqrt{\varepsilon}}}, \quad (36)$$

$$u \simeq \sqrt{\frac{G_{\perp}}{E_h}} (Y^* / \sqrt{\varepsilon}), \quad (37)$$

Scaling structures for the stress and deformation fields in Eqs. (36) and (37) are in accord with results in [7] (the stress or strain thus obtained is indeed anisotropic). In this

case, we can estimate the fracture energy  $\sigma u \simeq G_{\perp}$  via the maximum stress for a continuum stress ( $\sigma_F \simeq \sqrt{\sqrt{\varepsilon} G_{\perp} E_h / d}$ ) balancing with the yield stress of the pure aragonite ( $\sigma_{YS} \simeq \sqrt{E_h \gamma_h / a_h}$ ):  $G_{\perp} \simeq \lambda_{\perp} \gamma_h$  where  $\lambda_{\perp} = d / (\sqrt{\varepsilon} a_h) \gg 1$ ; the fracture energy is enhanced from that of the pure aragonite  $\gamma_h$  because  $a_h (\ll d)$  is a microscopic size of defects in a sample.

### III. INCLUSION OF VISCOELASTIC EFFECT

From the above scaling arguments, we have seen that  $u_y$  is a dominant component of the deformation field for parallel fractures while  $u_x$  is important for perpendicular fractures. Since  $u_y$  essentially corresponds to the deformation in soft layers while  $u_x$  to that in hard layers, viscoelastic effects associated with extremely soft layers becomes important only for parallel fractures; we shall include these effects into our theory.

As a model for viscoelasticity, we employ the simplest model (also utilized in [16]):

$$\mu(\omega) = \mu_0 + (\mu_{\infty} - \mu_0) \frac{i\omega\tau}{1 + i\omega\tau} \quad (38)$$

This is the minimal model to include the following essential properties of weakly cross-linked network: (1) its slow motions are governed by a weak-modulus  $\mu_0$  associated with weak cross-links, (2) its fast motions involve a strong-modulus  $\mu_{\infty} (\gg \mu_0)$  originating from entanglements.

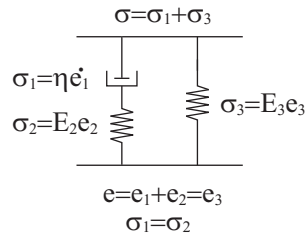


FIG. 3: Zener model with two springs and a dashpot.

This model is a special case of the Zener model (see Fig. 3), [17, 18] for which stress  $\sigma$  and strain  $e$  satisfy the relation,

$$\sigma + \frac{\eta}{E_2} \dot{\sigma} = E_3 e + \eta \frac{E_2 + E_3}{E_2} \dot{e} \quad (39)$$

with identification,  $E_3 = \mu_0$ ,  $E_2 = \mu_\infty - \mu_0$ , and  $\tau = \eta/E_2$ .

The previous purely elastic treatment should correspond to the zero frequency limit or the static limit of a viscoelastic model. For parallel fractures,  $(y, y)$  component of stress ( $\sigma$ ) is important, for which we write  $\sigma = \sigma_s \simeq E_s e_s$  where  $\sigma_s$  and  $e_s$  denote stress and strain of soft layers. Thus, it is natural to require that soft layers obey the trumpet relation  $\sigma_s + \tau \dot{\sigma}_s = \mu_0 e_s + \mu_\infty \tau \dot{e}_s$  with  $\mu_0 = E_s$ , because then the static limit reduces to the desired form. Noting the relations between coarse-grained stress and strain of nacre ( $\sigma$  and  $e$ ) and more local stress and strain of soft layers ( $\sigma_s$  and  $e_s$ ), i.e.  $\sigma = \sigma_s$  and  $e_s d_s = ed$ , we deduce a viscoelastic model for nacre:

$$\sigma + \tau \dot{\sigma} = E_0 e + E_\infty \tau \dot{e} \quad (40)$$

where

$$E_\infty = \lambda E_0 = \lambda E_s / \varepsilon_d \quad (41)$$

$$\tau = \frac{\eta}{\mu_\infty - \mu_0} \quad (42)$$

$$\lambda = \mu_\infty / \mu_0 \quad (43)$$

We note again that  $\mu_0 = E_s$  is associated with weak cross-links in soft layers, while  $\mu_\infty$  with entanglement in soft layers.

Putting  $\sigma = \sigma_m e^{i\omega t}$  and  $e = e_m e^{i\omega t}$ , with the definition of the viscoelastic modulus,  $\sigma_m = \mu(\omega) e_m$ , we obtain Eq. (38) with  $\mu_\infty$  and  $\mu_0$  replaced by  $E_\infty$  and  $E_0$ , respectively. This model can be divided into three regimes:

$$\begin{aligned} \text{I. } \omega\tau \ll 1/\lambda: & \quad \mu(\omega) \simeq E_0 \quad (\text{soft solid}) \\ \text{II. } 1/\lambda \ll \omega\tau \ll 1: & \quad \mu(\omega) \simeq i\omega\eta \quad (\text{liquid}) \\ \text{III. } 1 \ll \omega\tau: & \quad \mu(\omega) \simeq E_\infty \quad (\text{hard solid}) \end{aligned} \quad (44)$$

#### IV. CRACK SHAPE AND FRACTURE ENERGY

In the following we consider only large cracks:  $l \gg X$ . The opposite limit is examined in a separate article. [19] In the case of such large cracks, we are always in the isotropic regime where  $X \simeq Y (\equiv R)$  (see also Fig. 2a). We imagine a crack propagating at a constant speed  $V$ . For simplicity, we treat only certain large velocities:  $l \ll V\tau$ ; although it is very difficult

to estimate  $\tau$  for the protein, this corresponds to  $\tau \gg 10^{-2}$  s for  $l \simeq 100$   $\mu\text{m}$  and  $V \simeq 1$  cm/s.

An important observation here is the scaling identification of a distance  $r$  from the tip and the frequency  $\omega$  via a stationary crack-propagation speed  $V$ :

$$r \simeq V/\omega; \quad (45)$$

small distances correspond to high frequencies while long distances to low frequencies — the farther away from the tip, the more time for relaxation. Corresponding to Eq. (44), the fracture is spatially divided into three regions:

$$\begin{aligned} \text{I. } \lambda V\tau \ll r: & \quad \text{soft solid} \\ \text{II. } V\tau \ll r \ll \lambda V\tau: & \quad \text{liquid} \\ \text{III. } d \ll r \ll V\tau: & \quad \text{hard solid} \end{aligned} \quad (46)$$

Another important observation is that, in certain model of viscoelasticity, the scaling relation  $\sigma \sim r^{-1/2}$  (where  $r$  is a distance from the fracture tip) still holds as in a purely elastic model. This point shall be explained in next section.

First we consider a large crack size ( $L \gg \lambda V\tau$ ); then, all the three regions I-III are present. The soft-solid region I corresponds to low frequencies, and thus, to the static limit; in this region ( $r \gg \lambda V\tau \gg l$ ), Eqs. (25)-(27) holds. In the liquid zone II, the stress field scales as  $\sigma \simeq \omega\eta e \simeq \eta V u / r^2$  and at the same time it should scale as  $\sigma \sim r^{-1/2}$  from the above second observation. Thus, the strain should scale as  $u \sim r^{3/2}$  and the product as  $\sigma u \sim r$ . The coefficients can be determined by matching at  $r \simeq \lambda V\tau$ , i.e. the boundary between I and II: for example, we have

$$\sigma u \simeq G_{\parallel} \frac{r}{\lambda V\tau} \quad (\text{liquid zone}). \quad (47)$$

When we reach the hard solid region ( $r \simeq V\tau$ ), we find

$$\sigma u \simeq G_{\parallel} / \lambda \quad (\text{hard-solid zone}) \quad (48)$$

When we are in the solid region, as in the same manner (due to the simplifying condition  $l \ll V\tau$ ) with the derivation of Eqs. (25)-(27), we can show

$$\sigma \simeq \sqrt{G_0 E_{\infty} / R^*} \quad (49)$$

$$u \simeq \sqrt{G_0 R^* / E_{\infty}} \quad (50)$$

$$\sigma u \simeq G_0 \quad (51)$$

Here, we emphasize that  $G_0$  is associated with the hard solid appearing near the tip and is different from  $G_{\parallel}$  (At the place very close to the tip ( $r \ll l$ ), Eqs. (49)-(51) are no longer valid and they merge to the lenticular expressions [8]). From Eqs. (48) and (51), we find

$$G_{\parallel} \simeq \lambda G_0. \quad (52)$$

The overall separation energy  $G_{\parallel}$  is enhanced from  $G_0$  associated with the hard solid. The crack shape resulting from this analysis is just like a trumpet (see Fig. 4), as has been suggested by the name of the model. The similar form has been predicted [16] and observed [20] also in systems (weakly or non cross-linked polymers) rather different from the present anisotropic system.

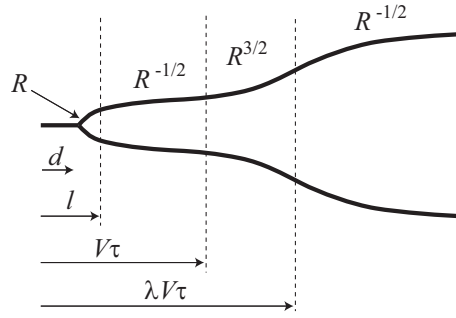


FIG. 4: Viscoelastic trumpet. The dependence of deformation field  $u$  on a distance from the tip  $R$  is indicated in the figure. Very close to the tip ( $l \ll R$ ), the shape merges to a lenticular form [8].

We complete our arguments by considering smaller fractures. When  $(l <)V\tau < L < \lambda V\tau$ , only the hard-solid and liquid regions are present; the soft solid has yet to develop. In this situation, the fracture energy is given by Eq. (47) at  $r = L$ :  $G_{\parallel}(V) = G_0 L / (V\tau)$ ; the toughness decreases with velocity. When  $(l <)L < V\tau$ , only the hard-solid region is developed and the fracture energy is given by  $G_0$ . Thus, as a function of  $V$ , the fracture energy starts from a larger plateau value  $\lambda G_0$ , and then decreases to reach a smaller plateau value  $G_0$ :

$$G_{\parallel}(V) = \begin{cases} \lambda G_0 & \text{for } d/\tau < V < L/(\lambda\tau) \\ G_0 L / (V\tau) & \text{for } L/(\lambda\tau) < V < L/\tau \\ G_0 & \text{for } L/\tau < V \end{cases} \quad (53)$$

Note here that in a continuum theory we only consider the region  $V\tau > d$ . This behavior

can be confirmed more precisely from a general formula [16]:

$$\frac{G_{\parallel}(V)}{G_0} \simeq E_{\infty} \int \frac{d\omega}{\omega} \text{Im} \left[ \frac{1}{\mu(\omega)} \right] \quad (54)$$

which can be analytically calculated for the trumpet model (just as in the previously known isotropic case [21]).

## V. DISCUSSION

In [16] the following observations are used: (A1) for a certain range of  $V$ , a (dimensional) dynamical equation  $\rho Dv/Dt = -\nabla\sigma$  for viscoelastic materials can be replaced by  $\nabla\sigma = 0$ , (A2) accordingly, in certain model of viscoelasticity, the scaling relation  $\sigma \sim r^{-1/2}$  still holds as in a purely elastic model, (A3) similar to the usual LEFM, we can expect a relation,  $\mathcal{G} \simeq K^2/E_{\infty}$  for certain viscoelastic models (where  $K$  and  $\mathcal{G}$  the stress intensity factor and the energy release rate associated with the tip), and (A4) we can find scaling structure of fracture energy from the product  $\sigma u$ , calculated at a large  $r$ . (Our arguments are, however, slightly different from the original one in that we did not explicitly use (A3).) We present possible interpretations for these observations to complement the original arguments.

Before showing our interpretations, we assume that the rheological relation is linear in a sense that the stress and strain are governed by

$$\sigma(t) = \int dt' E(t-t') \dot{e}(t') \quad (55)$$

In terms of Fourier transform (in time), this reduces to a simple *proportional relation*:

$$\sigma_{\omega} = \mu(\omega) e_{\omega} \quad (56)$$

where  $\mu(\omega) = i\omega E_{\omega}$ ;  $\mu(\omega)$  has the dimension of an elastic modulus  $E(t)$ . Here, we have used the notation  $O_{\omega} = \int dt O(t) e^{-i\omega t}$ . We shall use the scaling identification Eq. (45) in the following arguments.

### A. Interpretation for $\nabla\sigma = 0$

$\rho Dv/Dt = -\nabla\sigma$  can be dimensionally reexpressed in terms of Fourier components (in space and time) of stress and deformation as  $\rho\omega^2 u_{k,\omega} \simeq k\sigma_{k,\omega}$ . This equation reduces to

$V^2 u_{k,\omega} \simeq c^2 u_{k,\omega}$  for a linear rheology ( $\sigma_{k,\omega} \simeq E k u_{k,\omega}$ ) and for a crack propagation speed  $V$  ( $\omega \simeq V k$ , or Eq. (45)). Here, the sound velocity  $c$  is defined as  $c = \sqrt{E/\rho}$ . Thus, if  $V \ll c$ , we can neglect  $\rho Dv/Dt$  against  $\nabla\sigma$ . For  $E \simeq 10^5$  N/m<sup>2</sup> and  $\rho \simeq 10^3$  kg/m<sup>3</sup>,  $c \simeq 10$  m/s, which is sometimes high compared with typical crack propagation speeds, say, of cm/s.

### B. Interpretation for $\sigma \sim r^{-1/2}$

In the plane strain condition, there are only three independent stress components:  $\sigma_{xx}$ ,  $\sigma_{yy}$  and  $\sigma_{xy}$ . For  $V \ll c$ , we can start from  $\nabla\sigma = 0$ , which gives only two independent equations:  $\frac{\partial\sigma_{xx}}{\partial x} + \frac{\partial\sigma_{xy}}{\partial y} = 0$  and  $\frac{\partial\sigma_{yy}}{\partial y} + \frac{\partial\sigma_{xy}}{\partial x} = 0$ . The third equation is a compatibility equation, which directly follows from the definition (Eq. (7)):  $\frac{\partial^2 e_{xx}}{\partial y^2} + \frac{\partial^2 e_{yy}}{\partial x^2} = 2 \frac{\partial^2 e_{xy}}{\partial x \partial y}$ . Again, for a linear rheology, we have a simple proportional relation of the type  $\sigma_{ij} = E_{ijkl} e_{kl}$  or  $e_{ij} = D_{ijkl} \sigma_{kl}$  in Fourier space (in time only). Then, the three differential equations for Fourier component (in time) of  $\sigma_{ij}$  with respect to variables  $x$  and  $y$  have the same spacial scaling structure as in a purely elastic model where  $\sigma(t) = E(t)e(t)$ . Thus, the scaling structure,  $\sigma \sim r^{-1/2}$  should be unaltered even in a linear viscoelastic model.

### C. Interpretation for $\mathcal{G} \simeq K^2/E_\infty$ and scaling formula for fracture toughness $G \simeq \sigma u$

To establish  $\mathcal{G} \simeq K^2/E_\infty$  in the viscoelastic model and to understand why it can not be replaced by  $\mathcal{G} \simeq K^2/E_0$ , we start from the text book derivation [13]; we imagine that a crack is closed to a smaller size from the tip by applying a necessary work, say from a initial size  $a + \Delta a$  to a reduced size  $a$  (see Fig. 5).

The energy release rate  $\mathcal{G}$  (per unit length of crack front) is defined by

$$\mathcal{G} = \lim_{\Delta a \rightarrow 0} \frac{\Delta U}{\Delta a} \quad (57)$$

where the work of crack closure (per unit crack-front length) can be expressed as

$$\Delta U \simeq \int_{x=0}^{x=\Delta a} 2dx \int dy \int_e^0 (-\sigma) de \quad (58)$$

Here, the factor 2 counts both the upper and the lower sides of the crack.

This quantity depends on a history of closure process, for example, via Eq. (55). However, we will finally consider the limit  $\Delta a \rightarrow 0$  as in Eq. (57), while the relevant frequency is

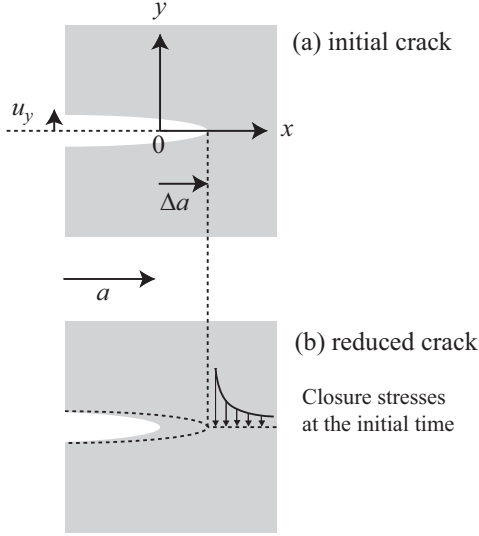


FIG. 5: Closure of a crack.

given by  $V/\Delta a$  ( $\rightarrow \infty$ ): very high frequency is important. In such a case, the trumpet model behaves as a solid with a modulus  $E_\infty$  ( $\sigma \simeq E_\infty e$ ). Namely,

$$\Delta U \simeq \int dx \int dy \sigma^2 / E_\infty. \quad (59)$$

As shown before, even in the trumpet model, we expect  $\sigma \simeq K/\sqrt{r}$ , if we denote the coefficient (the stress intensity factor) by  $K$ . Thus, Eq. (59) leads to  $\Delta U \simeq \Delta a K^2 / E_\infty$ ; we indeed recover  $\mathcal{G} \simeq K^2 / E_\infty$ . At the critical of failure, this corresponds to

$$G_0 \simeq K^2 / E_\infty \quad (60)$$

*The critical value of the energy release rate, which is the conventional fracture energy, is associated here with the hard solid region near the tip.*

We emphasize here that the overall fracture energy  $G_\parallel$  should scale as  $\lim_{\Delta a \rightarrow \infty} \frac{\Delta U}{\Delta a}$ , which is *different from the critical value of the energy release rate*. Then, in contrast with the limit  $\Delta a \rightarrow 0$ , very low frequency becomes important; we have to use  $\sigma \sim E_0 e$  in this context to find

$$G_\parallel \sim K^2 / E_0. \quad (61)$$

The stress intensity factor  $K$  in Eqs. (60) and (61) are actually different; these factors are an unknown coefficient for a known singularity ( $\sim \sqrt{r}$ ) in the above arguments. In fact,

from Eqs. (25) and (49), they are respectively given by  $\sqrt{G_0 E_\infty}$  and  $\sqrt{G_\parallel E_0}$ . In other words, Eqs. (60) and (61) can be directly reproduced from Eqs. (25) and (49).

Noting  $\Delta U \simeq \int dx \sigma(x)u(x)$  for linear models ( $\sigma \sim e$ ), we have an expression of the overall fracture energy  $G_\parallel$  for a *macroscopic*  $\Delta a$ :

$$G_\parallel \simeq \frac{1}{\Delta a} \int_0^{\Delta a} \sigma(x)u(x)dx \quad (62)$$

If the product  $\sigma(x)u(x)$  reaches a plateau value at a macroscopic distance  $x_0$ , we can expect a relation:

$$G_\parallel \simeq \sigma(x_0)u(x_0) \quad (63)$$

where the left-hand side is evaluated at a macroscopic distance  $x_0$  from the tip. This explains why we can use this product to estimate the fracture toughness, as announced in Sec. II. B (see, for example, Eq. (27)).

## VI. CONCLUSION

In this paper, we present physical pictures for fractures in nacre-type materials via scaling arguments, which is complementary to our previous more detailed analysis: strain distributions around a fracture are significantly different among (small and large) parallel and perpendicular fractures. From pictures thus obtained, we see that viscoelastic effects may play a role in parallel fractures and the effects are taken into account via the simplest model. We limit ourselves to the case of large cracks ( $X \gg l$ ) where crack-propagation speeds are not too slow ( $l \ll V\tau$ ); beyond this limit, crack shape and behavior of  $G(V)$  seems to be quite different, as discussed in a separate paper [19]. Within this limit, we found that the crack shape takes the trumpet form as in weakly (or non-) cross-linked polymers [20] although they are different in the region very close to the tip (this difference might be difficult to detect). The overall fracture energy  $G_\parallel$  is found to be enhanced from separation energy  $G_0$  associated with the hard solid region developed near the tip. It is emphasized that, here, the critical value of the energy release rate corresponds not to the overall fracture energy but a separation energy associated with the hard solid.

## Acknowledgments

The author (K.O.) is grateful to P.-G. de Gennes for useful discussions. K.O. also greatly appreciates Elie Raphaël and Florent Saulnier for discussions and for making their recent manuscript [21] available prior to submission. K.O. thanks members of group of P.G.G. at Collège de France, including David Quéré, for a warm hospitality during his third stay in Paris. This stay is financially supported by Collège de France.

## APPENDIX: ROUGH IMAGES AT THE SCALING LEVEL AND EXACT DISTRIBUTIONS

In order to clarify the meaning of physical pictures illustrated in Fig. 2, we give examples on comparison of such pictures with an exact solution available for perpendicular cracks (Figs. 6 and 7). We employ the following analytical expression [7]:

$$\sigma \sim e \sim \operatorname{Re} \left[ \frac{e^{i\pi z/(2L)}}{(e^{i\pi z/L} - 1)^{1/2}} \right] \quad (\text{A.1})$$

with  $z = x + iy/\sqrt{\varepsilon}$  where  $\varepsilon = 1$  and  $\varepsilon = 0.1$  for Figs. 6 and 7, respectively ( $L = 1$ ). This expression have separate length scales for  $x$ - and  $y$ -direction:  $L$  and  $L/\sqrt{\varepsilon}$ , respectively. Fig. 6 presents an example of the conventional isotropic sample ( $\varepsilon = 1$ ) while Fig. 7 an example of a perpendicular crack in a nacre-type material ( $\varepsilon = 0.1$ ).

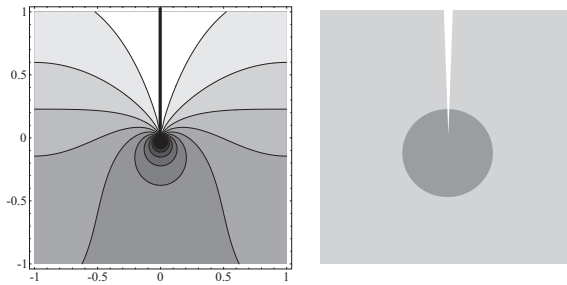


FIG. 6: Left: contour plot of strain distribution for a crack (size  $L$ ) in an isotropic elastic sample (the dimension  $2L \times 2L$ ) based on an analytical solution ( $\varepsilon = 1$ ). Here,  $L$  is the unit length. Right: corresponding physical image. The distribution is isotropic in a sense that there is only one length scale  $L$ .

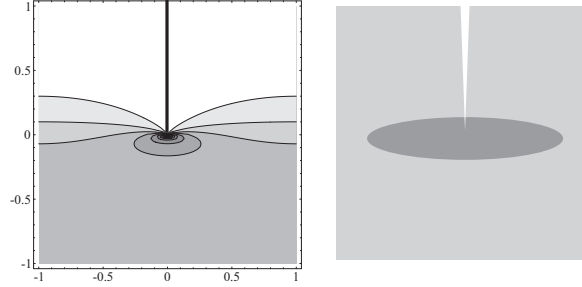


FIG. 7: Left: contour plot of strain distribution for a perpendicular crack (size  $L$ ) in a nacre-type elastic sample (the dimension  $2L \times 2L$ ) based on an analytical solution obtained in [7] ( $\varepsilon = 0.1$ ). Here again,  $L$  is the unit length. Right: corresponding physical image. The distribution is anisotropic in a sense that there is two separate length scales where the length scale for  $x$ -direction is  $L$  and that for  $y$ -direction is  $L/\sqrt{\varepsilon}$ .

In most experimental cases the crack size can be much smaller than the sample dimension. In such cases, detail analytical behaviors will change but physical pictures at the scaling level stays intact.

- 
- [1] T. Kelly and B. Clyne, *Physics Today* **52**, 37 (1999).
  - [2] William J. Clegg, *Science* **286**, 1097 (1999).
  - [3] *Biomimetics: Design and Processing of Materials*, edited by Ilhan A. Aksay, M. Sarikaya (AIP Press, New York, 1995).
  - [4] *Ceramic matrix composites: components, preparation, microstructure and properties*, edited by R. Naslain and B. Harris (Elsevier Applied Science, 1989).
  - [5] M. P. Rao, A. J. Sánchez-Herencia, G. E. Beltz, R. M. McMeeking, and F. F. Lange, *Science* **286**, 102 (1999).
  - [6] P.-G. de Gennes and K. Okumura, *C. R. Acad. Sci. Paris t.1, Ser. IV*, 257 (2000).
  - [7] K. Okumura and P.-G. de Gennes, *Eur. Phys. J. E* **4**, 121 (2001).
  - [8] K. Okumura, *Eur. Phys. J. E* **7**, 303 (2002).
  - [9] J. D. Currey, *Proc. R. Soc. Lond. B***196**, 443 (1977).
  - [10] A. P. Jackson, J. F. V. Vincent, and R. M. Turner, *Proc. R. Soc. Lond. B***234**, 415 (1988).

- [11] F. Song and Y. Bai, *J. Mater. Res.* 17 (2002) 1567.
- [12] A. G. Evans, Z. Suo, R. Z. Wan, I. A. Aksay, M. Y. He, and J. W. Hutchinson, *J. Mater. Res.* 16, 2475 (2001); R. Z. Wang, Z. Suo, A. G. Evans, N. Yao, and I. A. Aksay, *J. Mater. Res.* 16, 2485 (2001).
- [13] T. L. Anderson, *Fracture Mechanics — Fundamentals and Applications* (CRC Press, Boca Raton, 1991).
- [14] P. G. de Gennes, *Europhys. Lett.* 13, 709 (1990).
- [15] P. G. de Gennes, *The Physics of Liquid Crystal*, Clarendon Press (Oxford, London, 1974).
- [16] P. G. de Gennes, *Langmuir* 13, 4497 (1996); *C. R. Acad. Sci. Paris t. 307, Ser. II*, 1949 (1988); *C. R. Acad. Sci. Paris t. 312, Ser. II*, 1415 (1991); *Soft Interfaces* (Cambridge Univ. Press, 1997).
- [17] C.-Y. Hui, D.-B. Xu and E. J. Kramer, *J. Appl. Phys.* 72, 3294 (1992).
- [18] C. Oudet, "Polymères: structure et propriétés" (Masson, Paris, 1994).
- [19] K. Okumura, *Viscoelastic fractures in stratified composite materials: "lenticular trumpet,"* *Europhys. Lett.* (submitted).
- [20] T. Ondarçuhu, *J. Phys. II France* 7, 1893 (1997).
- [21] F. Saulnier, E. Raphaél, P.-G. de Gennes, and T. Ondarçuhu, in preparation.